Article

Development of a Control System for Underwater Vehicles with Multilink Manipulators Performing Contact Manipulation Operations

Alexander Konoplin, Nikita Krasavin *[ID], Alexander Yurmanov, Pavel Piatavin, Roman Vasilenko and Maxim Panchuk

Federal State Budgetary Institution of Science M. D. Ageev Institute of Marine Technology Problems, Far East Branch, Russian Academy of Sciences (IMTP FEB RAS), 690091 Vladivostok, Russia; konoplin@marine.febras.ru (A.K.); yurmanov@marine.febras.ru (A.Y.); piatavin@marine.febras.ru (P.P.); vasilenko@marine.febras.ru (R.V.); panchuk@marine.febras.ru (M.P.)
* Correspondence: nakrasavin@yandex.ru; Tel.: +7-(902)-506-30-14

Abstract: This article proposes a new method for the synthesis of autonomous underwater vehicles (AUVs) with a multilink manipulators control system, which provides for the automatic execution of contact manipulation operations by AUVs in stabilized hovering mode near or above target objects. To achieve the desired magnitude of the working tool's force effect on the object surface, the force vector exerted by this tool is calculated. Next, control signals providing additional movements of the manipulator's tool in the direction of the desired force vector are generated. Simultaneously, based on the calculated effects from the manipulator on the AUV, the thrusts of the latter's thrusters create the necessary pull at the manipulator's attachment point, which allows it to exert the desired force effects on the object surface. To compensate for the inevitable AUV stabilization system errors, leading to the tool's deviations from the trajectory, the latter is automatically corrected, taking into account the actual AUV deviations. As a result, contact manipulation operations are performed while maintaining the continuous contact of the tool with the object, even with slight displacements of the AUV from the stabilization point. The operability and efficiency of the synthesized system are confirmed by the results of numerical modeling, with the use of basin experimental data and visualization.

Keywords: autonomous underwater vehicle; multilink manipulator; position–force control; contact operations; stabilization system

1. Introduction

Currently, autonomous and hybrid underwater vehicles are increasingly equipped with multilink manipulators for a variety of applications—in particular, to perform various underwater research and technological operations in autonomous mode [1,2]. However, despite the fact that promising areas have been developing recently that do not require the physical contact of the AUV with objects of work—for example, so-called "sensor fields" [3,4]—most manipulation operations require the contact of the manipulator's working tool with the target objects [5–7]. Such operations can be both relatively simple (the collection of bacterial mats and sediment sampling) and relatively complex (the cleaning of surfaces suffering from fouling and silting, the insertion of samplers into control panels on underwater manifolds, etc.).

Research sampling operations require a sampler to be moved along a desired trajectory, with a specified orientation of this tool relative to the seabed surface. In this case, it is not necessary to exert a known force effect on the surface. However, for such operations as the cleaning of surfaces or interaction with underwater infrastructure objects, exerting a specified force on the surface of the object with the manipulator's working tool is important.

The most convenient and safe mode for performing these operations is the stabilized hovering mode of the AUV near or above the target object [1,8,9]. In this mode, the vehicle is holding the most convenient position for manipulation and does not stir up silt in the near-bottom layer of water, as happens when landing on the seabed. However, when the manipulator comes into contact with the surface of the object, a force begins to act on its working tool. This leads to undesirable external moments acting on the output shafts of the electric drives in the degrees of the manipulator's mobility, and also to force and moment effects on the point of the manipulator's attachment to the AUV. These impacts displace the AUV from its hovering point, which inevitably leads to deviations of the working tool from preset trajectories and loss of contact with the surface of the target object.

Currently, there are already solutions to the problem of providing position–force control of manipulators, including those installed on AUVs. For this, methods of parallel position–force control [10–12] or impedance control [13–17] are used. In the former case, to control the movements of the working tool, two control circuits of the manipulator drives are synthesized: by position and by the generated force. In turn, impedance control implies the formation of dependencies between the desired working tool's position and the force created by this tool at the point of contact with the target object. At the same time, it was noted in [18] that impedance control cannot be strictly attributed to either position or force control. There are also methods [19] that combine both of the above approaches in the force control of underwater manipulators. In many studies, it is proposed to use six-axis force and torque sensors to measure the dynamic effects on the AUV and the manipulator that occur when the latter comes into contact with the target object [20,21]. For example, in [22], the authors created a positional force control system for a hydraulic underwater manipulator of an ROV equipped with a six-axis sensor in the instrument. The method [23] made it possible to move the working tool of an underwater manipulator equipped with a force–torque sensor along a wall, with this tool exerting a specified force effect on its surface. The performance of the developed method was tested using a computer simulation. The method [10] is based on the use of an additional control loop for the AUV, which minimizes the coupling effects between the vehicle and the manipulator during contact operations. To make this method work, a torque sensor installed at the attachment point of the manipulator to the AUV was used. This made it possible to neutralize the emerging inaccuracies in the operation of the AUV navigation system. However, these studies did not take into account the specifics of the navigation system in underwater conditions and the associated delays in the formation of the AUV's vectors of deviation from a certain stabilization point.

Adaptive methods of impedance control of underwater manipulators were presented in [24,25], and in [25], a control system was built for a remote-controlled manipulator performing a contact operation. Both systems were investigated using computer modeling and showed high efficiency. In turn, the effectiveness of the control system developed in [26] was investigated during a basin experiment taking into account underwater currents. However, in these works [24–26], the bases of the manipulators were fixed while performing contact operations, and, accordingly, the inevitable deviations of the AUV from the stabilization point, which affect the quality of manipulation operations, were not taken into account.

In [27], two control schemes for the manipulator and the AUV for the implementation of force manipulation operations are considered: the first scheme implies the formation of additional thrusts and moments by the propellers of the AUV and the drives of the manipulator, respectively; the second implies the correction of the movement speeds of the manipulator links and the AUV. In both proposed systems, it is clearly seen from computer simulation results that during the execution of the contact operation, the manipulator practically does not change its position, maintaining its original configuration, and the movement of the tool is mainly ensured by an accurate displacement of the AUV. In reality, achieving such a precision of AUV movement is very difficult [28] due to its greater inertia compared to the manipulator, as well as the static characteristics of its thrusters. It can be seen from the graphs presented that the efficiency of the system decreases when additional

impact occurs on the tool in a direction perpendicular to the direction of action of the desired force.

At the same time, in many works [29–31], it was noted and shown during experiments and computer simulations that the use of six-axis force–torque sensors significantly complicates the practical implementation of the proposed methods for the following reasons: sensors are subject to noise; due to their design, they reduce the rigidity of the kinematic chain; they have a limited bandwidth; they have a high cost and imply changes in the design of the manipulator.

Approaches are also known to the position–force control of industrial manipulators that do not require force–torque sensors. For example, in works [31–35], the estimation of the force exerted on the manipulator tool was carried out with the help of observers and Kalman filters. The effectiveness of these approaches has been confirmed by numerical simulation [31,32] and experiments [33–35]. In particular, in studies [36,37], a method is proposed that allows the calculating of the desired values of external torques for each degree of mobility of multilink manipulators with an arbitrary kinematics, which together provide a given force effect of the working tool on target objects. Furthermore, correction devices have also been synthesized that allow simultaneously and accurately controlling the position of the output shaft of each electric drive of the manipulator and its external torque, through the simultaneous minimization of errors in these two components using a quadratic criterion. In study [29], observers were used for the force control of an industrial manipulator, providing information about the torque effects acting in the drives. However, these approaches are efficient only in cases where the base of the manipulator is not displaced relative to the target object, which cannot be achieved when performing operations in the hovering mode of an AUV. The approach proposed in [38] involves the creation of thrust at the attachment point of the manipulator by the AUV thrusters, which is necessary for the position–force control of a manipulator with a fixed base [36], while taking into account the peculiarities of the influence of a viscous fluid on the moving links of this manipulator. However, the practical use of this approach will be limited by the insufficient accuracy of the stabilization of the AUV [39] due to the inertia of the vehicle, the nonlinearity of the static characteristics of its thrusters and the limited accuracy of determining the displacements of the AUV relative to the object by means of the technical vision systems (TVS), as well as delays in obtaining navigation information.

In turn, in works [30,40–42], fuzzy algorithms and neural networks were used to evaluate the contact force. However, the use of such intelligent algorithms greatly complicates the system, since it requires the selection and configuration of many parameters, such as the number of layers and nodes of the neural network, the types of activation functions, the number and types of fuzzy rules and membership functions. Also, training and debugging such algorithms is a time-consuming process.

It is important to note that in many works, the calculation of the inverse of the Jacobian is often required, which can slow down the operation of the entire system [18], since, often, the computing power of on-board computers is limited. In addition, the calculation of the inverse of the Jacobian can lead to computational problems when approaching degenerate positions or boundaries of the manipulator's working area [30].

Thus, the conclusion can be drawn that the known methods and approaches still do not provide a high performance of common contact manipulation operations in the AUV's hovering mode. Therefore, in the present study, we aimed to develop a new control system for AUVs equipped with multilink manipulators to perform contact operations, devoid of the above disadvantages.

The remainder of this paper is organized as follows. Section 2 briefly describes the methods used in the work, as well as describing the kinematic scheme of the AUV with manipulator considered in the work. The essence of the proposed method is described in detail in Section 3. Section 4 presents the results of a semi-realistic modeling of the control system, synthesized on the basis of the proposed method using data obtained during the basin experiment. Section 5 provides a discussion of the simulation results

obtained. Section 6 summarizes all of the work and also provides plans for further work by the authors.

2. Specifics of Underwater Contact Operations and Methods Used

Before performing an underwater contact operation using system [8] based on point clouds obtained from the onboard TVS of the AUV, the target object is identified, and the desired trajectory of the manipulator's working tool is transferred onto its surface, taking into account the possible silting, fouling, and deformation of the object. In this case, the orientation of the working tool is set based on the triangulation surface of the object formed, taking into account the requirements for performing the specific operation. After that, the AUV takes a spatial position near the object. In this object, the trajectory of the working tool is located in the working area of the manipulator in such a way that this tool approaches the object's surface at a certain service angle. This condition ensures the manipulator will exert minimal possible dynamic effects on the AUV when coming in contact with the surface, and also allows it to compensate for undesirable displacements of the AUV by changing its configuration. To perform research manipulation operations, this problem is addressed in [43].

To be stabilized in the desired spatial position above or near the target object, the AUV should have a propulsion layout that controls the movements of the vehicle along six degrees of freedom by its thrusters. An example of such a layout for the thrusters of an AUV equipped with a multilink manipulator is shown in Figure 1. To provide the movement of the working tool with a certain orientation within the working area, the manipulator must have at least six degrees of mobility. As an example, consider the kinematic configuration of a PUMA manipulator with six degrees of mobility (Figure 1) attached under the center of the buoyancy of the vehicle, which allows for the minimizing of the dynamic effects on the AUV during operations of this manipulator. However, to perform manipulations with vertical structures, the manipulator can be mounted to the side of the vertical axis of the vehicle.
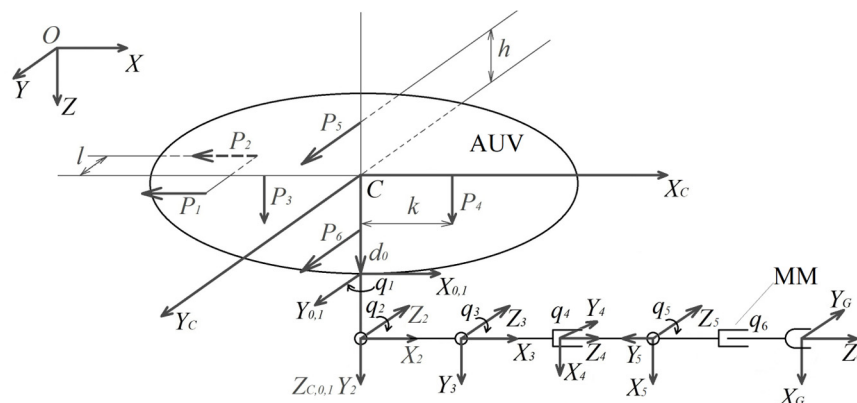

Figure 1. Kinematic configuration of AUV with manipulator; MM is multilink manipulator.

In Figure 1, the designations are as follows: $OXYZ$ is the absolute coordinate frame (CF) in which the AUV moves; $CX_CY_CZ_C$ is the CF rigidly related to the AUV's hull, the beginning of which is located at the center C of the buoyancy of the vehicle, the axis CX_C coincides with the horizontal–longitudinal axis of the AUV, the axis CZ_C coincides with its vertical axis and is directed downward, and the CY_C axis makes up the right-hand triple with them; $X_0Y_0Z_0$ is the CF related with the base of the manipulator; $X_1Y_1Z_1$, $X_2Y_2Z_2$, ..., $X_5Y_5Z_5$ are the CF constructed using one of the most efficient varieties of the Denavit–Hartenberg approach [44,45] and are related with the origins of the respective links of the manipulator; $X_GY_GZ_G$ is the CF related with the working tool of the manipulator; q_1, q_2, ..., q_6 are the generalized coordinates of the manipulator; P_1, P_2, ..., P_6 are the thrusts created by the AUV's thrusters; h, l, k are the geometric

parameters of the layout of the AUV's thrusters; and $d_0 \in R^3$ is the vector determining the position of the manipulator's base in the CF $CX_CY_CZ_C$.

The stabilization of the AUV in the hovering mode is provided by a combined system [46] consisting of closed and open control loops. The open loop compensates for the negative dynamic effects from the manipulator moving in a viscous medium by the thrusters of the vehicle. The force and moment effects of the manipulator on the AUV are calculated using a recurrent algorithm for solving the inverse dynamics problem (IDP) modified for an underwater multilink manipulator [47], taking into account the specifics of the effects of a viscous medium on its links. The closed-loop stabilization subsystem holds the AUV in a certain spatial position based on information about the actual linear and angular displacements of this vehicle. The angular displacements of the AUV are estimated by the onboard gyroscopes; linear displacements, by the visual navigation systems [48,49].

To compensate for the unavoidable errors of the AUV stabilization system which cause the manipulator's working tool to shift from the preset trajectory, it is necessary to automatically correct the programmed trajectories and orientation of this tool by means of the system [50], taking into account the actual displacements of the AUV relative to the initial position. The use of this system will allow the manipulator's working tool to move along the surface of the target object, maintaining continuous contact with this surface, even with inevitable (albeit insignificant) displacements of the AUV from the stabilization point under the effect of the reaction force exerted by the surface of the object on the working tool.

Since many research manipulation operations do not require a specified force to act on the target object's surface and are performed after achieving the desired positions of the working tool and the target surface relative to each other, it is sufficient to use the above-described AUV stabilization systems [46] and make corrections of the manipulator's programmed trajectories [50] and orientation to perform such operations. However, the force acting on the working tool upon contact with the object leads to undesirable external moments on the output shafts of the manipulator's electric drives in the degrees of mobility. These moments lead to errors in the positioning of the working tool and should be compensated for by means of additional control signals of the respective electric drives of the manipulator, formed by adaptive corrective devices [47].

3. Description of the Method for the Force Control of an AUV with a Manipulator

To perform contact operations with an AUV in the stabilized hovering mode with the manipulator exerting the desired force effect on the object, a method is proposed that does not require high-cost and bulky six-axis force–torque sensors and the resource-consuming calculation of the Jacobian inverse. This method consists of three stages implemented simultaneously in real time.

At the first stage, as the manipulator's working tool is smoothly approaching the surface of the target object, during the contact movement along this surface, the external moments are estimated that act on the output shafts of the manipulator's drives in all degrees of mobility as a result of the specified force contact. Based on the estimated values of external moments for the manipulator's specific kinematic configuration, the magnitude and direction of the vector of force exerted by the manipulator's working tool on the target object during the contact operation are calculated.

At the second stage, based on information about the desired and actual vectors of force applied to the surface of the object, control signals are sent to the manipulator's drives of all degrees of mobility. These signals provide extra movements of the working tool in the direction that ensures achievement of the desired magnitude of force effect of this tool on the surface of the target object. In addition, when undesirable linear and angular displacements of the AUV from the initial position appear, the configuration of the manipulator is corrected [50] in such a way that the specified position and orientation of the working tool relative to the surface of the stationary object are maintained. As a result, such a double correction ensures the continuous contact of the moving tool with the surface

of the target object, even with inevitable delays in obtaining information about the linear displacements of the AUV relative to the target object, as well as with the limited accuracy of the position closed-loop stabilization subsystem of the vehicle.

At the third stage, control signals are sent to the inputs of the AUV's respective thrusters to compensate for the dynamic effects from the manipulator moving in a viscous medium on this vehicle and exerting a force on the target object. Moreover, the control signals of the AUV's thrusters are formed in real time on the basis of analytical expressions that estimate the force and torque that this manipulator exerts on the AUV. To do this, the calculated magnitude and direction of the vector of the force exerted by the manipulator's working tool on the target object, the effects of mutual influence between all degrees of mobility of the manipulator, and also the hydrostatic and hydrodynamic forces of resistance to its movement, including viscous frictions and the added masses of the surrounding fluid [51,52], are taken into account. As a result, the AUV is accurately stabilized in the hovering mode near or above the target object during the manipulator's operation. This creates the necessary pull at the point of the manipulator's attachment to the AUV, which allows the working tool of this manipulator to exert the desired force effects on the surface of the target object.

It should be noted that, when performing the most critical operations, the movement of the working tool along the trajectory should begin only after achieving the desired force effect of this tool on the target object at the start point of the trajectory.

The proposed method is implemented as follows. When the working tool of the underwater manipulator is moving along the surface of the target object, an external moment $^{i}M_{dz}$, directed along the axis of the hinge i, acts on the output shaft of the manipulator's gear drive of the i-th degree of mobility ($i = \overline{1,n}$, where n is the number of degrees of mobility of the manipulator):

$$^{i}M_{dz} = {}^{i}M_{wz} + {}^{i}M_{ez} \tag{1}$$

Here, $^{i}M_{wz}$ is the moment caused by the mutual effects between all degrees of mobility of the manipulator, and also by the hydrostatic and hydrodynamic forces of resistance to its movement, including viscous friction and the added masses of the surrounding fluid; and $^{i}M_{ez}$ is the moment caused by the support reaction force of the target object's surface $^{G}\vec{F}_{e}$, which is equal in magnitude and opposite in direction to the force of the working tool's impact on this object—$^{G}\vec{F}_{imp} \in R^{3}$.

Figure 2 shows the above-listed vectors of the forces and moments, and also the vectors of the force $^{C}\vec{F} \in R^{3}$ and moment $^{C}\vec{M} \in R^{3}$ effects on the AUV from the moving manipulator. The ^{G} index marks the vectors associated with the manipulator's working tool, specified in the CF $X_{G}Y_{G}Z_{G}$.

As already noted above, the right CF with $X_{i}Y_{i}Z_{i}$ is rigidly related to each link of the manipulator. The $^{i}M_{dz}$ value is measured using a relatively simple one-axis joint torque sensor [53] or an observer of the drive load moment [29,47]. Thus, values of $^{i}M_{wz}$ moments are calculated using the analytical expressions of the IDP solution for the underwater manipulator [47]. The magnitude of the $^{i}M_{ez}$ moment is calculated using the expression:

$$^{i}M_{ez} = {}^{i}M_{dz} - {}^{i}M_{wz} \tag{2}$$

Afterwards, the components of the vector of force acting on the manipulator's tool $^{G}\vec{F}_{e}$ are determined for a specific kinematic configuration of the manipulator, using the calculated values of external moments $^{i}M_{ez}$ acting on the output shafts of the drives in all degrees of mobility, as a result of the force contact of this manipulator's working tool with the surface of the target object. To simplify the description of the proposed method, it is sufficient to consider the four degrees of mobility (three portable and one orienting) of a PUMA-type manipulator with $q_{4} = q_{6} = 0$ (Figure 2). For the accepted kinematic configuration of an underwater multilink manipulator, the calculation of the above-mentioned vector is as follows.
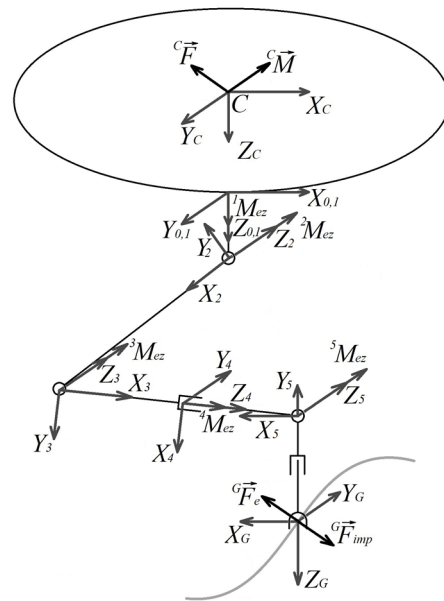
Figure 2. An AUV performing a contact operation; direction vectors of forces and moments acting in the case of a working tool's contact with the surface of the target object.

It is obvious that with $^G\vec{F}_e \neq 0$ in the joint of the fifth degree of the manipulator's mobility, an additional moment of force arises. Taking into account $q_6 = 0$, this moment is calculated using the following recurrent ratios [47]:

$$^5\vec{M}_e = {}^5\vec{p} \times ({}_G^5 A\, {}^G\vec{F}_e) = \begin{bmatrix} 0 \\ {}^5p_y \\ 0 \end{bmatrix} \times \left(\begin{bmatrix} 1 & 0 & 0 \\ 0 & 0 & -1 \\ 0 & 1 & 0 \end{bmatrix} \begin{bmatrix} {}^G F_{ex} \\ {}^G F_{ey} \\ {}^G F_{ez} \end{bmatrix} \right) = \begin{bmatrix} {}^G F_{ey}\, {}^5p_y \\ 0 \\ -{}^G F_{ex}\, {}^5p_y \end{bmatrix} \quad (3)$$

where $^i\vec{p} \in R^3$ is the vector directed along the longitudinal axis of link i and determining the position of the CF related with link $i + 1$ in the CF of the i-th link; $_{i+1}^i A \in R^{3\times3}$ is the rotation matrix of vectors from the CF related with link $i + 1$ into the CF related with the base of the i-th link; ($\times$) is a vector product of vectors.

The moment $^5\vec{M}_e$ component $^5M_{ez}$ directed along the pivot axis of the joint will have an effect on the output shaft of the manipulator's gear drive of the fifth degree of mobility. Therefore, taking into account expression (3), the component $^G F_{ex}$ of the force $^G\vec{F}_e$ acting along the X_G axis can be found using the expression:

$$^G F_{ex} = -\frac{^5M_{ez}}{^5p_y} \quad (4)$$

The components $^G F_{ez}$, $^G F_{ey}$ of the vector $^G\vec{F}_e$ acting on the manipulator's working tool are calculated in a similar way, on the basis of the measured values of the moments $^3M_{ez}$ and $^1M_{ez}$ arising in the drives of the third and first degrees of mobility, respectively, and caused by the effect of the vector $^G\vec{F}_e$ on the working tool. For the kinematic configuration of the manipulator used, the vector $^3\vec{F}_e$, taking into account the direction of the CF axes located in the manipulator's degrees of mobility and with $q_4 = 0$, will have the following form:

$$\vec{^3F}_e = {^3_5A}\,\vec{^5F}_e = {^3_5A}\left({^5_GA}\,\vec{^GF}_e\right) = \begin{bmatrix} -s_5 & -c_5 & 0 \\ c_5 & -s_5 & 0 \\ 0 & 0 & 1 \end{bmatrix}\left(\begin{bmatrix} 1 & 0 & 0 \\ 0 & 0 & -1 \\ 0 & 1 & 0 \end{bmatrix}\begin{bmatrix} {^GF}_{ex} \\ {^GF}_{ey} \\ {^GF}_{ez} \end{bmatrix}\right) =$$

$$= \begin{bmatrix} -s_5 & -c_5 & 0 \\ c_5 & -s_5 & 0 \\ 0 & 0 & 1 \end{bmatrix}\begin{bmatrix} {^GF}_{ex} \\ -{^GF}_{ez} \\ {^GF}_{ey} \end{bmatrix} = \begin{bmatrix} {^GF}_{ez}c_5 - {^GF}_{ex}s_5 \\ {^GF}_{ez}s_5 + {^GF}_{ex}c_5 \\ {^GF}_{ey} \end{bmatrix} \tag{5}$$

where $c_5 = \cos(q_5)$, $s_5 = \sin(q_5)$.

In this case, taking into account (3) and (5), the vector $\vec{^3M}_e$ will have the following form:

$$\vec{^3M}_e = \vec{^3p} \times \vec{^3F}_e + {^3_5A}\,\vec{^5M}_e = \begin{bmatrix} {^3p}_x \\ 0 \\ 0 \end{bmatrix} \times \begin{bmatrix} {^GF}_{ez}c_5 - {^GF}_{ex}s_5 \\ {^GF}_{ez}s_5 + {^GF}_{ex}c_5 \\ {^GF}_{ey} \end{bmatrix} +$$

$$+ \begin{bmatrix} -s_5 & -c_5 & 0 \\ c_5 & -s_5 & 0 \\ 0 & 0 & 1 \end{bmatrix}\begin{bmatrix} {^GF}_{ey}{^5p}_y \\ 0 \\ -{^GF}_{ex}{^5p}_y \end{bmatrix} = \begin{bmatrix} -{^GF}_{ey}{^5p}_y s_5 \\ {^GF}_{ey}({^5p}_y c_5 - {^3p}_x) \\ {^3p}_x({^GF}_{ex}c_5 + {^GF}_{ez}s_5) - {^GF}_{ex}{^5p}_y \end{bmatrix} \tag{6}$$

Based on (6), it is easy to calculate:

$$^3M_{ez} = {^3p}_x({^GF}_{ex}c_5 + {^GF}_{ez}s_5) - {^GF}_{ex}{^5p}_y,$$

which makes it possible, taking into account expression (4), to express ${^GF}_{ez}$ as follows:

$$^GF_{ez} = \frac{{^3M}_{ez} - {^GF}_{ex}({^3p}_x c_5 - {^5p}_y)}{{^3p}_x s_5} = \frac{{^3M}_{ez} + \frac{{^5M}_{ez}}{{^5p}_y}({^3p}_x c_5 - {^5p}_y)}{{^3p}_x s_5} \tag{7}$$

The vector $\vec{^2M}_e$ in the CF related with the base of the second link of the manipulator is calculated as follows:

$$\vec{^2M}_e = \vec{^2p} \times \left({^2_3A}\,\vec{^3F}_e\right) + {^2_3A}\,\vec{^3M}_e = \begin{bmatrix} {^2p}_x \\ 0 \\ 0 \end{bmatrix} \times \begin{bmatrix} {^GF}_{ez}c_{35} - {^GF}_{ex}s_{35} \\ {^GF}_{ez}s_{35} + {^GF}_{ex}c_{35} \\ {^GF}_{ey} \end{bmatrix} +$$

$$+ \begin{bmatrix} c_3 & -s_3 & 0 \\ s_3 & c_3 & 0 \\ 0 & 0 & 1 \end{bmatrix}\begin{bmatrix} -{^GF}_{ey}{^5p}_y s_5 \\ {^GF}_{ey}({^5p}_y c_5 - {^3p}_x) \\ {^3p}_x({^GF}_{ex}c_5 + {^GF}_{ez}s_5) - {^GF}_{ex}{^5p}_y \end{bmatrix} = \tag{8}$$

$$= \begin{bmatrix} {^GF}_{ey}({^3p}_x s_3 - {^5p}_y s_{35}) \\ {^GF}_{ey}({^5p}_y c_{35} - {^3p}_x c_3 - {^2p}_x) \\ {^GF}_{ex}({^3p}_x c_5 - {^5p}_y + {^2p}_x c_{35}) + {^GF}_{ez}({^3p}_x s_5 + {^2p}_x s_{35}) \end{bmatrix}$$

where $c_{35} = \cos(q_3 + q_5)$, $s_{35} = \sin(q_3 + q_5)$.

Taking into account (8), we find the vector $\vec{^1M}_e$ in the CF related with the base of the first link of the manipulator:

$$
\begin{aligned}
{}^1\vec{M}_e = {}^1\vec{p} \times {}^1\vec{F}_e + {}^1_2 A\, {}^2\vec{M}_e &= \begin{bmatrix} 0 \\ 0 \\ {}^1p_z \end{bmatrix} \times \begin{bmatrix} {}^G F_{ez} c_{235} - {}^G F_{ex} s_{235} \\ -{}^G F_{ey} \\ {}^G F_{ez} s_{235} + {}^G F_{ex} c_{235} \end{bmatrix} + \\
&+ \begin{bmatrix} c_2 & -s_2 & 0 \\ 0 & 0 & -1 \\ s_2 & c_2 & 0 \end{bmatrix} \begin{bmatrix} {}^G F_{ey}({}^3 p_x s_3 - {}^5 p_y s_{35}) \\ {}^G F_{ey}({}^5 p_y c_{35} - {}^3 p_x c_3 - {}^2 p_x) \\ {}^G F_{ex}({}^3 p_x c_5 - {}^5 p_y + {}^2 p_x c_{35}) + {}^G F_{ez}({}^3 p_x s_5 + {}^2 p_x s_{35}) \end{bmatrix} = \\
&= \begin{bmatrix} {}^G F_{ey}({}^1 p_z - {}^5 p_y s_{235} + {}^3 p_x s_{23} + {}^2 p_x s_2) \\ {}^G F_{ez}({}^1 p_z c_{235} - {}^3 p_x s_5 - {}^2 p_x s_{35}) + {}^G F_{ex}({}^5 p_y - {}^3 p_x c_5 - {}^2 p_x c_{35} - {}^1 p_z s_{235}) \\ {}^G F_{ey}({}^5 p_y c_{235} - {}^3 p_x c_{23} - {}^2 p_x c_2) \end{bmatrix}
\end{aligned} \tag{9}
$$

where $c_{235} = \cos(q_2 + q_3 + q_5)$, $s_{235} = \sin(q_2 + q_3 + q_5)$.

Based on (9), it is easy to calculate:

$$
{}^1 M_{ez} = {}^G F_{ey}({}^5 p_y c_{235} - {}^3 p_x c_{23} - {}^2 p_x c_2) \tag{10}
$$

which makes it possible to express:

$$
{}^G F_{ey} = \frac{{}^1 M_{ez}}{{}^5 p_y c_{235} - {}^3 p_x c_{23} - {}^2 p_x c_2} \tag{11}
$$

Taking into account (4), (7) and (11), we find the result as follows:

$$
{}^G \vec{F}_e = \begin{bmatrix} {}^G F_{ex} \\ {}^G F_{ey} \\ {}^G F_{ez} \end{bmatrix} = \begin{bmatrix} -\dfrac{{}^5 M_{ez}}{{}^5 p_y} \\ \dfrac{{}^1 M_{ez}}{{}^5 p_y c_{235} - {}^3 p_x c_{23} - {}^2 p_x c_2} \\ \dfrac{{}^3 M_{ez} + \frac{{}^5 M_{ez}}{{}^5 p_y}({}^3 p_x c_5 - {}^5 p_y)}{{}^3 p_x s_5} \end{bmatrix} \tag{12}
$$

To ensure that the manipulator tool continuously exerts the desired force effect $\vec{F}^*_{imp} \in R^3$ on the surface of the work object, it is necessary to generate additional control signals for the degrees of mobility of this manipulator. These signals will provide additional tool movements to achieve the desired magnitude of force effect. This is achieved as follows.

Initially, at each point of the trajectory, a unit vector of the desired direction of action of force $\vec{k} \in R^3$, $\|\vec{k}\| = 1$, is set. Let us consider the case when, during the manipulation operation, at each moment of time, the manipulator's working tool is located at right angles to the tangent to the surface of the object at each point of the trajectory. Taking into account the previously obtained ratios (12), there is a difference between the desired vector $\vec{F}^*_{imp}$ and the projection of the actual acting vector $\vec{F}_{imp} \in R^3$ onto vector $\vec{k}$:

$$
\Delta \vec{F}_{imp} = \vec{F}^*_{imp} - \vec{k} \vec{k}^T \vec{F}_{imp}, \quad \vec{F}_{imp} = -\vec{F}_e \tag{13}
$$

The location of these vectors is shown in Figure 3. Taking into account (13), the required value of the additional tool offset is formed using the PID controller:

$$
\tilde{x} = K_p \Delta F + K_i \int \Delta F(\tau) d\tau + K_d \frac{d}{dt} \Delta F \tag{14}
$$

where K_p, K_i, K_d are the corresponding coefficients of the controller; and $\Delta F = \|\Delta \vec{F}_{imp}\| sign$ is the scalar value of the current difference between the values of the desired and actual

forces. This scalar difference is calculated taking into account the direction of the $\Delta \vec{F}_{imp}$ vector, determined by the value of angle α between vectors $\Delta \vec{F}_{imp}$ and $\vec{F}^*_{imp}$ (Figure 3):

$$\alpha = \arccos\left(\frac{\Delta \vec{F} \vec{F}^*_{imp}}{\|\Delta \vec{F}\|\|\vec{F}^*_{imp}\|}\right), \quad \begin{cases} if \ |\alpha| < \frac{\pi}{2} \Rightarrow sign = 1 \\ else \Rightarrow sign = -1 \end{cases} \tag{15}$$
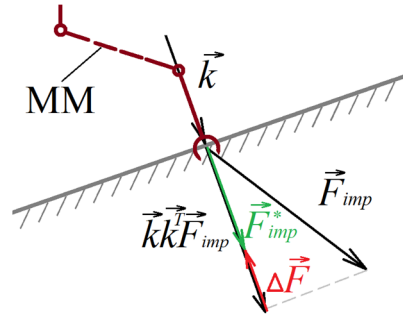
Figure 3. The directions of action of the acting vectors during the process of ensuring the continuous provision of a given force effect $\vec{F}^*_{imp}$; MM is the multilink manipulator.

As a result, taking into account the above, it is not difficult to obtain the desired $\Delta \vec{P}^* \in R^3$ vector of the additional displacement of the manipulator tool:

$$\Delta \vec{P}^* = \tilde{x} \vec{k} \tag{16}$$

It is important to note that in the above example of calculating vector $^G\vec{F}_e$ (12) is relevant for one of the many possible configurations of the manipulator (Figure 2) and was chosen to demonstrate the proposed calculation method. To accurately calculate vector $^G\vec{F}_e$, other possible configurations must be taken into account during the operation of the manipulator. These calculations are carried out in a similar way to expressions (3)–(12) and are not given in detail in order to preserve the required volume of the article, but are briefly described below.

In general, when the manipulator is not in any of the special positions, vector $^G\vec{F}_e$ is calculated based on information about the moments $^5M_{ez}$, $^4M_{ez}$, $^3M_{ez}$. If $q_5 = 0$, $q_4 \neq 0$, $q_3 \neq 0$, then the calculation of $^G\vec{F}_e$ is based on the moments $^5M_{ez}$, $^3M_{ez}$, $^2M_{ez}$. If $q_5 = 0$, $q_4 = 0$, $q_3 \neq 0$, $q_2 \neq 0$, then $^G\vec{F}_e$ is calculated based on $^3M_{ez}$, $^2M_{ez}$, $^1M_{ez}$.

To create the necessary pull at the manipulator's attachment point to the AUV, which will allow the working tool of this manipulator to exert the desired force effects on the surface of the target object, signals are to be sent to the inputs of the respective AUV thrusters. This will compensate for the force and moment effects exerted on this AUV by the manipulator.

To create additional control signals for the AUV thrusters in real time, the vectors of the force $^C\vec{F}$ and moment $^C\vec{M}$ of the manipulator's actions on the AUV's center of displacement are calculated (Figure 2). These vectors are determined by the magnitude and direction of the vector $^G\vec{F}_e$ (12) of force exerted on the manipulator's working tool by the target object, by the mutual effects between all the manipulator's degrees of mobility, and also by the hydrostatic and hydrodynamic forces of resistance to the movement of the links, including viscous friction and the added masses of the surrounding fluid: $^G\vec{F}_D \in R^3$, $^C\vec{M}_D \in R^3$, respectively. The above-mentioned dynamic effects $^C\vec{F}$ and $^C\vec{M}$, taking into

account the calculated value $^G\vec{F}_e$ (12), are estimated using analytical expressions describing the solution of the manipulator's IDP [47].

According to the layout of the axes of the manipulator links' CF and to expression (12), the vectors of force and moment from the manipulator that act on the AUV are calculated as follows:

$$^C\vec{F} = {}^C\vec{F}_D + {}^C_G A \, {}^G\vec{F}_e, \quad {}^C\vec{M} = {}^C\vec{M}_D + {}^C\vec{M}_e \tag{17}$$

where $^C\vec{M}_e \in R^3$ is the moment due to the force $^G\vec{F}_e$; and $^C_G A \in R^{3\times3}$ is the rotation matrix of vectors from the CF $X_G Y_G Z_G$ related with the manipulator's working tool into the AUV's CF $CX_C Y_C Z_C$.

The calculated effects are compensated for by the respective AUV thrusters using an open loop of the stabilization system [46]. As a result, the AUV is stabilized in the hovering mode near or above the target object while its manipulator is performing operations. The necessary pull is created at the point of the manipulator's attachment to the AUV, which allows the working tool of this manipulator to exert the desired force effects on the surface of the object.

However, even with above-mentioned stabilization system, the AUV will have small inevitable displacements from its stabilization point. These displacements will lead to the loss of force contact of the manipulator's tool with the surface of the object. To compensate for these small displacements and keep the tool on its trajectories, an automatic correction of the programmed trajectories and orientation of the manipulator's tool is required.

The corrected vectors of the position and orientation of the manipulator's working tool $\vec{P}^* \in R^3$, $\vec{X}_G^*$, $\vec{Y}_G^* \in R^3$ represented in the CF $CX_C Y_C Z_C$, taking into account the linear and angular displacements of the AUV, will have the following form:

$$^C\vec{P}^* = {}^O_C R^T\left(\vec{P}^* - \vec{r}\right) \quad {}^C\vec{X}_G^* = {}^O_C R^T \vec{X}_G^*, \quad {}^C\vec{Y}_G^* = {}^O_C R^T \vec{Y}_G^* \tag{18}$$

where $^O_C R = R^{3\times3}$ is the rotation matrix of the CF $CX_C Y_C Z_C$ relative to CF $OXYZ$; and $\vec{r} \in R^3$ is the vector of the AUV linear displacement in the CF $OXYZ$.

It should be noted that to avoid chattering during the transient phase while establishing the contact of the manipulator's tool with the object surface, the tool's approach speed should be maintained as relatively low.

A block diagram of the control system synthesized on the basis of the proposed method is shown in Figure 4. The new acronyms used in this figure are as follows:

- TCU is the unit for correcting the trajectory and orientation of the manipulator's working tool [50];
- MM and its CS is the model of a multilink manipulator and its control system [47];
- AUV SS is a stabilization system that forms the resulting thrust vector $\vec{T} = [P_1, P_2, \ldots, P_6]^T$ created by the AUV thrusters to compensate for the vector $\vec{G}$ of external force and torque effects on this vehicle from sea currents and the moving manipulator;
- AUV NS is the navigation system of the AUV that provides information about the current linear displacement vector $\vec{r}$ in the absolute CF $OXYZ$ and the angles of the AUV's roll, pitch, and yaw;
- FCU is the unit for controlling the force action exerted by the manipulator on the surface of the target object;
- ICU is the unit for calculating the current interaction force of the manipulator with the surface of the object;
- IDP is the unit of the IDP solution for the underwater manipulator;
- $\vec{F}_{ext}$ is the vector of external forces acting on the links and the working tool of the manipulator, caused by its interaction with the surrounding viscous medium and the surface of the target object;

- $\vec{P} \in R^3$ is the vector of the actual position of the working tool.
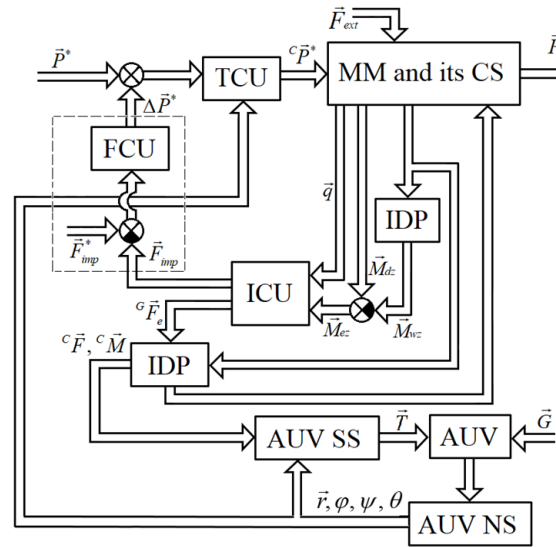

Figure 4. Block diagram of developed control system for AUV with manipulator.

4. Results of Semi-Realistic Simulation of System Operation

For the modeling in Matlab/Simulink R2018a, a well-tested mathematical model of AUVs [54] was used, with a multilink manipulator whose kinematic configuration is shown in Figure 1. The main parameters of the AUV and the manipulator are shown in Table 1. A complete list of parameters of the AUV model used is provided in [8]; a manipulator model and its parameters are described in detail in [47]. In this case, the vector d_0 in the CF $CX_CY_CZ_C$ has the coordinates $d_0 = (0, 0, 0.35)^T$ (Figure 1).

Table 1. Parameters of AUV and its manipulator.

Parameters		Values (Unit)
AUV	L × W × H, m^3	1.2 × 1.5 × 0.9
	Weight, kg	170
	Gravity center, m	$[0, 0, 0.05]^T$
Link 1	Length, m	0.05
	Weight, kg	0.4
	Diameter, m	0.1
	Added mass, kg	0.1
	Viscous friction coeff.	0.6
Links 2, 3	Length, m	0.5
	Weight, kg	4
	Diameter, m	0.1
	Added mass, kg	1.075
	Viscous friction coeff.	0.6
Link 4	Length, m	0.15
	Weight, kg	0.5
	Diameter, m	0.08
	Added mass, kg	0.3
	Viscous friction coeff.	0.6

The model consists of a combined AUV stabilization system in the hovering mode [46], including an open loop (17), and a system [50] that allows the finding of the coordinates of the vector in the CF $CX_CY_CZ_C$ that determines the current desired position and orientation of the working tool on the surface of the object, using information about the linear and angular displacements of the AUV from its initial position (18). Moreover, the information

used by these systems about the angular displacements of the AUV, measured by the onboard gyroscopes, is obtained without time delays in the simulation. The vector $\vec{r}$ of the current linear displacements of the AUV relative to the stabilization point is formed with a delay of 0.25 s due to the speed of processing of the data received from the TVS.

To compensate for the external moments leading to errors in the positioning of the working tool that occur at the output shafts of the manipulator's gear drives and are caused by its movement in a viscous medium with a force acting on the target object, adaptive corrective devices are used [47].

To visualize the simulation process in the CoppeliaSim simulator, a seabed scene, including an AUV equipped with a manipulator, was reconstructed (Figure 5).
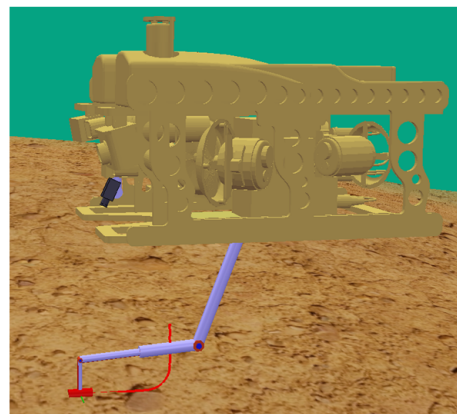
Figure 5. A soil sampling scene in the CoppeliaSim simulator.

A study of the quality of the synthesized system was carried out for two types of contact operations, which most clearly show the scope of application of this system.

The first case is an example of the simplest contact operation of soil sampling, using a sampling device installed in the end-effector of the manipulator. This type of work often involves the vertical or horizontal (as in the presented case) introduction of a sampler into the sediment layer of the soil in order to further study its composition. Such an operation is more straightforward, since it does not require the provision of a given force on the surface. When performing soil sampling, the most important thing is to maintain the relative position of the manipulator tool (sampler) and the surface of the work object (soil) in the case of force contact between them.

In the second case, the operation of cleaning an object of complex shape, previously identified with the help of TVS, is simulated. This operation, in addition to maintaining the specified orientation of the tool relative to a curved surface, requires the provision of a specified force action on this surface. This force's magnitude and direction should be determined by the technical requirements for a specific force operation.

To simulate the process of performing sampling operations that do not require a desired force acting on the seabed surface, a trajectory of the working tool was formed that simulated the sampling of the surface sediment layer (Figure 5). The manipulator guided the sampler along the seabed at a speed of 0.02 m/s. Also, during the modeling, the assumption was made that the soil at the sampling site had a homogeneous structure, and its surface was a horizontal plane.

At the moment of contact of the sampler with the sediment, a force with a vector opposite to the direction of the tool's movement began to act on the working tool. As a result of this contact, moments $^{2,3,5}M_{ez}$ appeared in the corresponding drives of the manipulator, the graphs of the changes of which are shown in Figure 6.
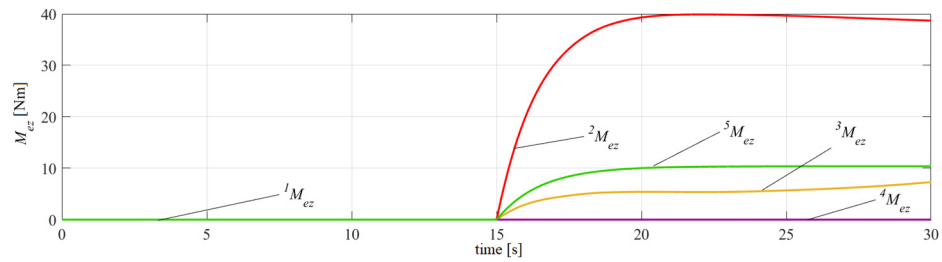
Figure 6. Moments in manipulator drives during soil sampling.

Taking into account the identified moments in the manipulator drives (Figure 6), the vector of force action $^G\vec{F}_e$ was calculated using expression (12), the obtained components of which are shown in Figure 7. From this figure, it can be seen that the identified value of the component of the $^G\vec{F}_{ex}$ vector directed against the motion of the sampler varied from 0 to 70 N. At the same time, it can be noted that the manipulator tool was also affected by the $^G\vec{F}_{ez}$ component, due to the reaction force of the support as a result of its partial immersion in the soil surface.
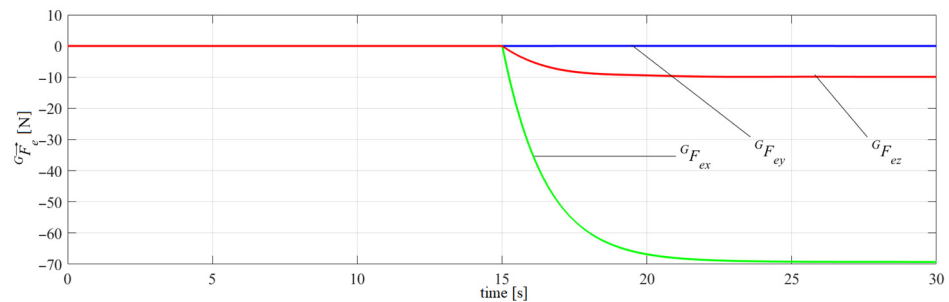

Figure 7. Components of the $^G\vec{F}_e$ force vector acting on the manipulator tool during soil sampling.

The identified components of the $^G\vec{F}_e$ vector (Figure 7) made it possible to compensate for the effects of the manipulator on the AUV using the open loop of the stabilization system (17). At the same time, the position and orientation of the manipulator tool was corrected based on the navigation data of the AUV (18). This made it possible to maintain the sampler with the specified orientation relative to the surface.

Figure 8 clearly shows that at 15 s, the angular and linear deviations of the AUV from the stabilization point increased significantly. These deviations were caused by the occurrence of contact of the sampler with the soil surface, as well as delays in obtaining visual navigation information from the TVS. At the same time, it can also be seen from the figure that, even taking into account the presence of angular and linear deviations of the AUV (Figure 8, $\|\vec{r}\|$, φ, θ, ψ), the Euclidean norm of the vectors of linear deviations of the manipulator (Figure 8, $\|\vec{e}\|$) did not exceed its permissible values.
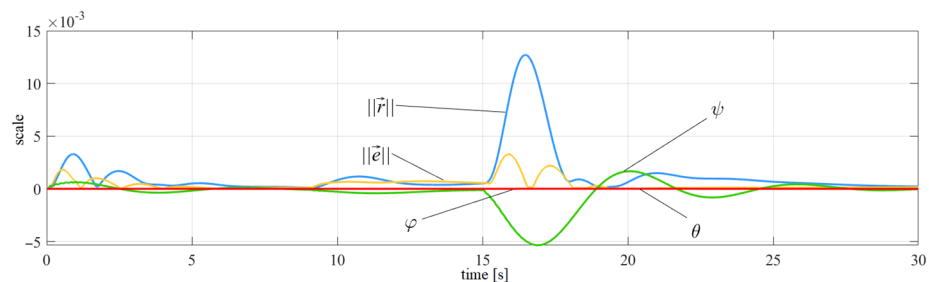

Figure 8. Results of simulation of sampling operation: $\|\vec{r}\|$, $\|\vec{e}\|$ = scale, m; φ, θ, ψ = scale, rad.

The process of cleaning the surface of an underwater object having a complex shape, with a manipulator's working tool applying a specified force and using experimental data, was also simulated. To do this, a PET bottle with a diameter of 0.35 m (Figure 9a) was placed in the testing pool to a depth of 1.5 m. Also, a TVS in a sealed box (Figure 9b) [55], developed at IMTP FEB RAS, was immersed in the pool. The TVS included a StereoLabs ZED2 stereo camera (San Francisco, USA), calibrated for operation in an aqueous environment, and an Nvidia Jetson computer (Silicon Valley, California, USA) that processed the received point clouds. After that, the scanning and recognition of the mentioned object was carried out using the TVS.
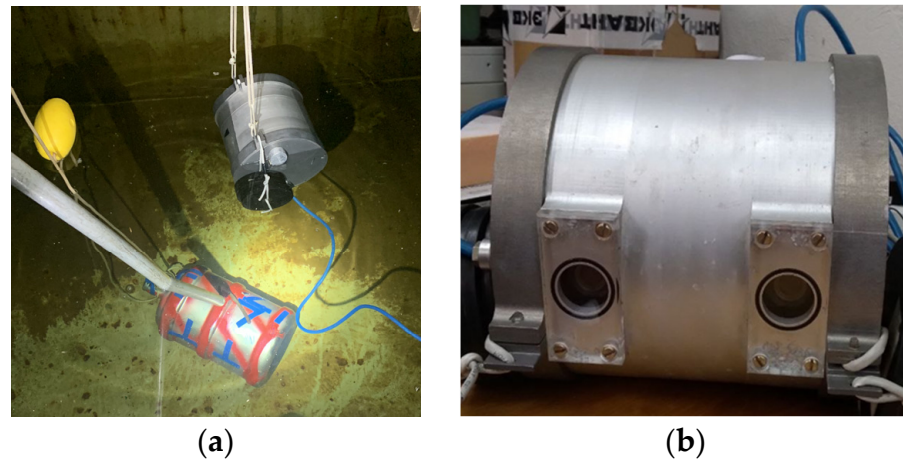

Figure 9. A TVS and the work object: (**a**) a test pool with the object of work and TVS submerged in it; (**b**) a stereo camera-based TVS in a sealed box.

The point cloud obtained as a result of scanning, containing the object of manipulation, is shown in Figure 10a,b.
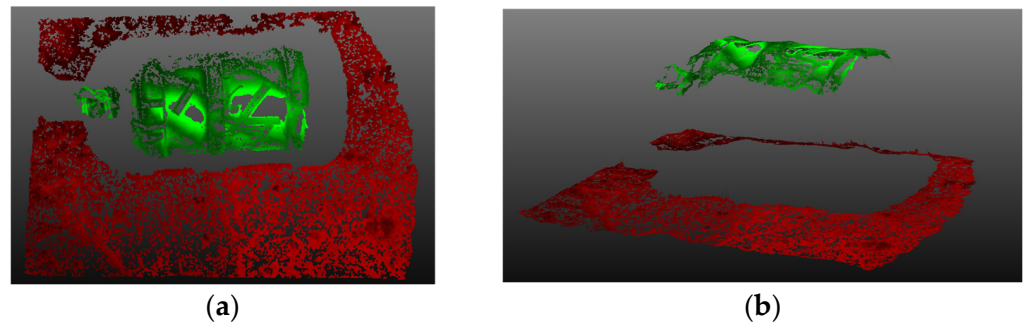

Figure 10. The point cloud obtained during underwater photography (red is the soil surface, green is the scanned object): (**a**) top view; (**b**) side view.

Then, using the well-known methods of RANSAC [56], Euclidean Cluster Extraction [57] and Iterative Closest Points [58], the object of work was selected from the resulting general point cloud of the scene by combining the point clouds of objects contained in the scene (highlighted in green in Figure 10) with the point cloud of the reference object. At the same time, in order to increase the accuracy of alignment, those points that could not be contained in the point cloud of a real object due to the unidirectional nature of scanning were discarded from the reference point cloud. After that, the accuracy of the alignment of the two point clouds was evaluated. For this purpose, method [59] was used, which consists in projecting special test trajectories onto the combined triangulation surfaces of the real object and its reference model. After that, the quadratic deviation between the corresponding points of these trajectories is calculated, on the basis of which the accuracy of the performed combination of the two point clouds is estimated.

As a result of the experiment, the target object, the bottle, was successfully identified based on the point clouds of the scanned scene (Figure 9a). At the same time, the error in determining the location of the object did not exceed 5 mm when it was located at a distance of 1 m from the TVS.

Then the desired trajectory was projected onto the triangulation surface of the scanned real bottle (Figure 10) perpendicular to its longitudinal axis (Figure 11a), and the fouling cleaning operation, with movement along it, was simulated. In Figure 11a, the purple and green surfaces are, respectively, the surfaces of the reference and scanned objects (Figure 10). The formed trajectory was sent to Matlab/Simulink to be tested by a dynamic model of the manipulator installed on the AUV in the force control mode. The simulation of the identified bottle cleaning also was visualized in CoppeliaSim (Figure 11b), where the triangulation model of the reference object was used. The speed of the tool's movement was 0.02 m/s. The coefficient of surface elasticity $\widetilde{k}$ was equal to $1 \cdot 10^4$ N/m. To control the magnitude of the exerted force, a controller (14) with coefficients $K_p = 1 \cdot 10^{-5}$, $K_i = 4 \cdot 10^{-4}$, $K_d = 4 \cdot 10^{-9}$ was used.
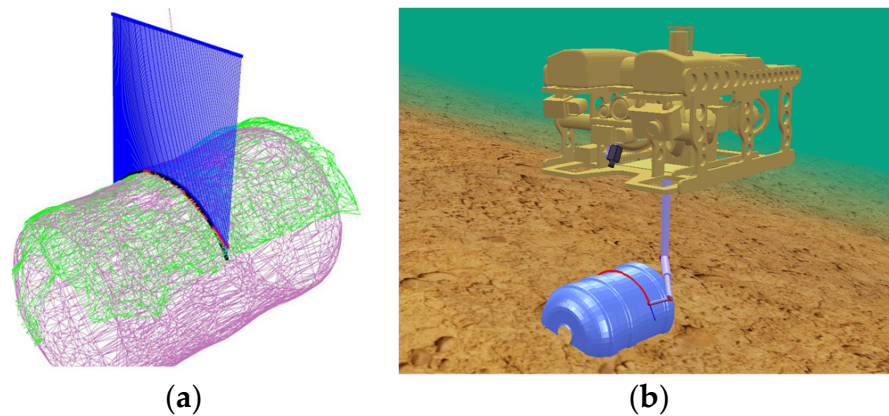

(**a**) (**b**)

Figure 11. Performing an operation to clean up an object of complex shape: (**a**) the scanned object and projected trajectory; (**b**) an object-cleaning operation in the CoppeliaSim 4.1.0. simulator.

During the operation, the manipulator guided its tool along the surface of the bottle, while maintaining its preset orientation perpendicular to the tangent to the surface at each point of the trajectory. During the process of this movement, a given force of 60 N was exerted on the surface of the bottle. Figure 12 shows graphs of the changes in the generalized coordinates of the manipulator during the bottle-cleaning operation. In turn, Figure 13 illustrates the identified components of the moments in the corresponding drives of the manipulator due to the action of the $^G\overrightarrow{F}_e$ vector on its tool. It is worth noting that moments identification errors did not exceed 0.5 Nm for all drives during the operation.
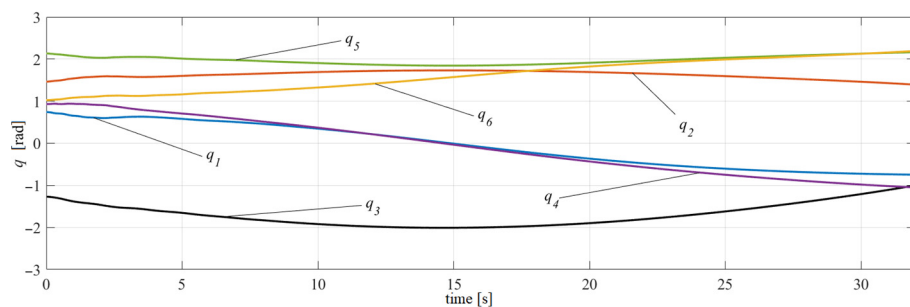

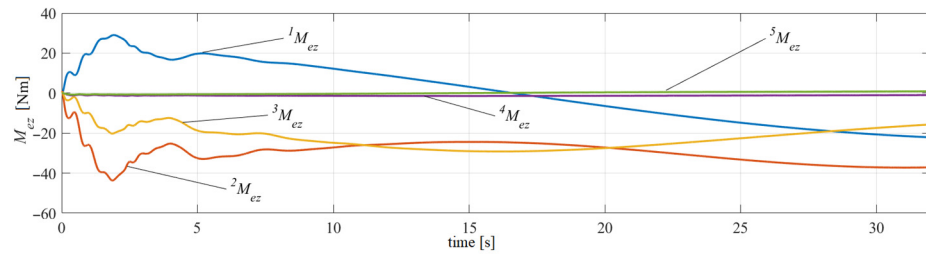**Figure 12.** Graphs of changes in the generalized coordinates of the manipulator.

Figure 13. Moments in the manipulator drives caused by the force contact of the tool with the surface of the object.

The components of the $^{G}\vec{F}_e$ vector, calculated taking into account the identified $^{i}M_{ez}$ moments (Figure 13), are shown in Figure 14. From this graph, it can be seen that after the completion of all transients, the manipulator tool acted on the object of work with a given force (Figure 14, $^{G}F_{ez}$). The same figure shows the $^{G}F_{ex}$ component due to the friction force of the tool with the surface of the processed bottle. The presented results show the absence of significant chattering between the working tool and the object of work, leading to periodic losses of force contact or to the complete impossibility of performing such operations.
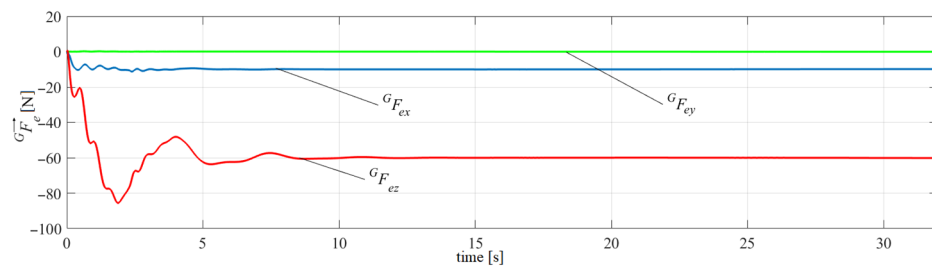

Figure 14. Components of the $^{G}\vec{F}_e$ force vector acting on the manipulator tool during the bottle-cleaning process.

Figure 15 shows the curves of variations in Euclidean norms $\|\vec{e}\|$, $\|\vec{r}\|$ vectors of the working tool's deviation from the specified trajectory and the deviation of the AUV center of displacement from the stabilization point in the absolute CF, and deviations of the AUV roll, pitch and yaw angles. As can be seen from the curves, at the beginning of the simulation, the vector $^{G}\vec{F}_e$ began to exert an effect on the working tool. However with the use of the calculated values $^{C}\vec{F}$, $^{C}\vec{M}$ in the open loop of the AUV stabilization system, which take into account the value of the calculated vector $^{G}\vec{F}_e$, the $\|\vec{r}\|$ deviation of the vehicle remained within 0.01 m in most parts of the simulation, while the value $\|\vec{e}\|$ did not exceed a few mm all along the trajectory.
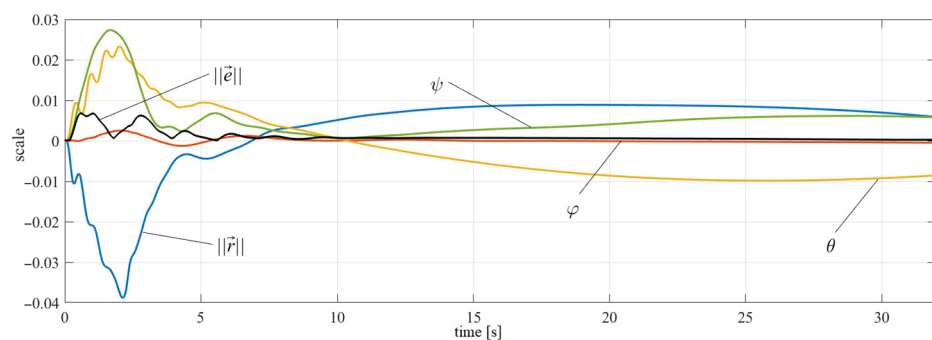

Figure 15. Results of simulation of cleaning operation: $\|\vec{r}\|$, $\|\vec{e}\| =$ scale, m; φ, θ, $\psi =$ scale, rad.

It should be noted that the increasing errors in the position and orientation of the AUV (Figure 15) that occur at the beginning of the simulation are due to several factors, such as delays in receiving navigation information from the TVS and the limited accuracy of the AUV propulsion control system, including the dynamic and static characteristics of its thrusters. These factors inevitably lead to an increase in the duration of transients during the establishment of a given force effect on the object of work (Figures 13 and 14). At the same time, the effectiveness of the control system for the force exerted by the manipulator (Figure 4) depends not only on the parameters of the controllers of the AUV stabilization system, but also on the selected coefficients of equation (14).

5. Discussion

The results of the numerical simulation allow the conclusion that the developed control system for AUVs equipped with multilink manipulators can be successfully used to perform contact manipulation operations. The practical implementation of this system will not cause fundamental difficulties and does not require expensive six-axis force–torque sensors.

It should also be noted that the studies of the proposed method for performing contact operations by an AUV with a manipulator confirmed the possibility of the manipulator's impact on the objects of work, with a given magnitude and direction of the force vector, in the mode of AUV stabilized hovering. Despite the fact that the studies were carried out using a typical PUMA-type manipulator kinematics, the developed method is applicable to any other manipulator kinematics. The influence of the friction force caused by the movement of the working tool on the surfaces of the object is compensated for by adaptive correcting devices of the manipulator drives. As a result, the required accuracy of the tool movement along the specified trajectories is provided, which was demonstrated in the process of numerical modeling.

The maintenance of the continuous contact (elimination of chattering) of the manipulator working tool with the surfaces of the objects of work was achieved, due to the proposed double correction of the position and orientation of this tool. At the same time, errors in the formation of manipulator trajectories along the surfaces of underwater objects due to the limited accuracy of the TVS calibration and the changing parameters of the aquatic environment were compensated for. This correction is implemented, taking into account information about the current linear and angular displacements of the AUV from its initial position, as well as information about the current magnitude and direction of the vector of force exerted by the working tool on the object.

6. Conclusions

In the present article, we propose a new method for an AUV with a manipulator to perform contact operations by exerting the desired force effect on the target object in the mode of stabilized hovering. The control system of these dynamic objects, synthesized on the basis of the method, does not require six-axis force–torque sensors and the resource-consuming calculation of the Jacobian inverse. This system calculates the magnitude and direction of the force vector exerted by the manipulator's working tool on the object during the operation. The information used for calculations are the external moments acting on the output shafts of the manipulator's gear drives in all degrees of mobility as a result of the force contact of the working tool with the surface of the object, measured by relatively simple one-axis sensors or estimated by observers.

The manipulator continuously exerts a specified force effect on the object through the additional displacement of the working tool in the direction of the vector of difference between the vectors of the desired and actual force effects. As the results of the numerical simulation have shown, for precisely controlling the force, it is sufficient to use a PID controller of the value $\Delta \vec{P}^{*}$ for the additional displacement of the tool.

Simultaneously, the thrusts of the AUV, formed by the open loop of its stabilization system, provide compensation for the real-time force and torque effects on the AUV from the manipulator performing the force operation. As a result, the necessary pull is created at

the point of the manipulator's attachment to the AUV, which allows the working tool of this manipulator to exert the desired force effects on the surface of the target object.

It is worth noting that the successful control of an AUV with a manipulator during a contact operation requires the contours of stabilization and correction of the trajectories and the orientation of the manipulator's working tool that are closed in the position and orientation of the vehicle. This allows continuous contact with the surface to be maintained all along the trajectory of the tool.

To test the operability and functional features of the synthesized system, a numerical simulation using experimental data was performed. The simulation took into account the dynamic characteristics of the AUV and the manipulator, and also the delays in obtaining information from the navigation system of the vehicle using the TVS. It is worth noting that for the numerical simulation, real information about the object of manipulation work obtained during an experiment with a real TVS was used. During the simulation, the deviations of the AUV from the stabilization point did not exceed 0.013 m and 0.04 m for the sampling and cleaning operations, respectively. In the first case, the magnitude of the force effect of the tool on the surface reached 70 N. In the second case, the manipulator successfully reached the set value of the force effect of 60 N, and the overshoot did not exceed 85 N. In both cases, the tool deviations from the trajectory did not exceed 0.006 m. The simulation results have confirmed the high efficiency of the proposed system in performing contact manipulation operations.

It is worth noting that when performing some of the most crucial manipulation work, a given effort must be exerted, starting from the point of first contact of the tool with the object of work. In this case, it is necessary that the tool remains stationary at the starting point of the trajectory, until all transients are completed during the establishment of a given force, and only after that does it begin to move along the trajectory.

At the same time, it is obvious that the effectiveness of the developed system largely depends on the accuracy of identifying moments in the manipulator drives caused by contact with the object of work. This is because the accuracy of determining these values depends on the accuracy of identifying the force exerted by the tool, which in turn affects the efficiency of the open loop of the AUV stabilization system.

It is expected that the use of the created methods will allow one not only to achieve a high-quality solution to currently existing operational tasks in offline mode, but also to significantly expand the range of work performed by the AUV. These developments formed the basis for the creation of experimental samples of underwater manipulators [60] and TVSs at the IMTP of the Far Eastern Branch of the Russian Academy of Sciences, which are based on the MMT-3500 AUV [61]. Further research will be aimed at developing docking technology using the proposed system, which will allow the automatic docking of AUVs equipped with manipulators with docking platforms. This method will include the capture of a universal rod mounted on the docking platform using a manipulator grip, followed by the docking of the AUV by automatically changing the configuration of the manipulator. It is also planned to conduct marine tests of the developed systems.

Author Contributions: Conceptualization, A.K.; methodology, A.K. and N.K.; writing—original draft preparation, A.K. and N.K.; software, data curation, A.Y., R.V., M.P. and P.P.; formal analysis, N.K.; investigation, N.K.; writing—review and editing, A.K., N.K., A.Y. and P.P.; visualization, N.K., A.Y., R.V., M.P. and P.P.; project administration, validation, supervision and funding acquisition, A.K. All authors have read and agreed to the published version of the manuscript.

Institutional Review Board Statement: Not applicable.

Informed Consent Statement: Not applicable.

Data Availability Statement: Upon request to the corresponding author of this article.

Conflicts of Interest: The authors declare no conflicts of interest.

References

1. Antonelli, G. Springer Tracts in Advanced Robotics. In *Underwater Robots*, 3rd ed.; Springer: Dordrecht, The Netherlands, 2014; p. 294. [CrossRef]
2. Cieslak, P.; Ridao, P.; Giergiel, M. Autonomous Underwater Panel Operation by GIRONA500 UVMS: A Practical Approach to Autonomous Underwater Manipulation. In Proceedings of the IEEE International Conference on Robotics and Automation (ICRA), Seattle, WA, USA, 26–30 May 2015; pp. 529–536. [CrossRef]
3. Hou, X.; Wang, J.; Bai, T.; Deng, Y.; Ren, Y.; Hanzo, L. Environment-Aware AUV Trajectory Design and Resource Management for Multi-Tier Underwater Computing. *IEEE J. Sel. Areas Commun.* **2023**, *41*, 474–490. [CrossRef]
4. Khan, J.; Cho, H. A Distributed Data-Gathering Protocol Using AUV in Underwater Sensor Networks. *J. Sens.* **2015**, *15*, 19331–19350. [CrossRef] [PubMed]
5. Simetti, E. Autonomous underwater intervention. *Curr. Robot. Rep.* **2020**, *1*, 117–122. [CrossRef]
6. González-García, J.; Gómez-Espinosa, A.; Cuan-Urquizo, E.; García-Valdovinos, L.G.; Salgado-Jiménez, T.; Escobedo Cabello, J.A. Autonomous underwater vehicles: Localization, navigation, and communication for collaborative missions. *Appl. Sci.* **2020**, *10*, 1256. [CrossRef]
7. Aldhaheri, S.; De Masi, G.; Pairet, È.; Ardón, P. Underwater robot manipulation: Advances, challenges and prospective ventures. In Proceedings of the 2022 OCEANS'22, Chennai, India, 21–24 February 2022; pp. 1–7. [CrossRef]
8. Konoplin, A.; Yurmanov, A.; Krasavin, N.; Piatavin, P. Development of a control system for multilink manipulators on unmanned underwater vehicles dynamically positioned over seabed objects. *Appl. Sci.* **2022**, *12*, 1666. [CrossRef]
9. Vu, M.T.; Le Thanh, H.N.N.; Huynh, T.T.; Thang, Q.; Duc, T.; Hoang, Q.D.; Le, T.H. Station-keeping control of a hovering over-actuated autonomous underwater vehicle under ocean current effects and model uncertainties in horizontal plane. *IEEE Access* **2021**, *9*, 6855–6867. [CrossRef]
10. Lapierre, L.; Fraisse, P.; Dauchez, P. Position/force control of an underwater mobile manipulator. *J. Robot. Syst.* **2003**, *20*, 707–722. [CrossRef]
11. Raibert, M.H.; Craig, J.J. Hybrid position/force control of manipulators. *J. Dyn. Syst. Control* **1981**, *103*, 126–133. [CrossRef]
12. Barbalata, C.; Dunnigan, M.W.; Petillot, Y. Coupled and decoupled force/motion controllers for an underwater vehicle-manipulator system. *J. Mar. Sci. Eng.* **2018**, *6*, 96. [CrossRef]
13. Cao, H.; Chen, X.; He, Y.; Zhao, X. Dynamic Adaptive Hybrid Impedance Control for Dynamic Contact Force Tracking in Uncertain Environments. *IEEE Access* **2019**, *7*, 83162–83174. [CrossRef]
14. Chien, M.C.; Huang, A.C. Adaptive Impedance Control of Robot Manipulators based on Function Approximation Technique. *Robotica* **2004**, *22*, 395–403. [CrossRef]
15. Kang, S.H.; Jin, M.; Chang, P.H. A solution to the accuracy/robustness dilemma in impedance control. *IEEE/ASME Trans. Mechatron.* **2009**, *14*, 282–294. [CrossRef]
16. Farivarnejad, H.; Moosavian, S.A.A. Multiple impedance control for object manipulation by a dual arm underwater vehicle–manipulator system. *Ocean Eng.* **2014**, *89*, 82–98. [CrossRef]
17. Hogan, N. Impedance control: An approach to manipulation. In Proceedings of the 1984 IEEE American Control Conference, San Diego, CA, USA, 6–8 June 1984; pp. 304–313. [CrossRef]
18. Izadbakhsh, A.; Khorashadizadeh, S. Robust impedance control of robot manipulators using differential equations as universal approximator. *Int. J. Control* **2017**, *91*, 2170–2186. [CrossRef]
19. Anderson, R.J.; Spong, M.W. Hybrid impedance control of robotic manipulators. *IEEE J. Robot. Autom.* **1988**, *4*, 549–556. [CrossRef]
20. Cetin, K.; Zapico, C.S.; Tugal, H.; Petillot, Y.; Dunnigan, M.; Erden, M.S. Application of adaptive and switching control for contact maintenance of a robotic vehicle-manipulator system for underwater asset inspection. *Front. Robot. AI* **2021**, *8*, 706558. [CrossRef]
21. Cieślak, P.; Ridao, P. Adaptive admittance control in task-priority framework for contact force control in autonomous underwater floating manipulation. In Proceedings of the 2018 IEEE/RSJ International Conference on Intelligent Robots and Systems (IROS), Madrid, Spain, 1–5 October 2018; pp. 6646–6651. [CrossRef]
22. Dunnigan, M.W.; Clegg, A.C.; Edwards, I.; Lane, D.M. Hybrid position/force control of a hydraulic underwater manipulator. *IEE P-Contr. Theor. Ap.* **1996**, *143*, 145–151. [CrossRef]
23. Cui, Y.; Yuh, J. A unified adaptive force control of underwater vehicle-manipulator systems (UVMS). In Proceedings of the 2003 IEEE/RSJ International Conference on Intelligent Robots and Systems, Las Vegas, NV, USA, 27–31 October 2003; pp. 553–558. [CrossRef]
24. Zhang, J.; Li, H.; Liu, Q.; Li, S. The model reference adaptive impedance control for underwater manipulator compliant operation. *Trans. Inst. Meas. Control* **2023**, *45*, 2135–2148. [CrossRef]
25. Zhang, J.; Xia, M.; Li, S.; Liu, Z.; Yang, J. The adaptive bilateral control of underwater manipulator teleoperation system with uncertain parameters and external disturbance. *Electronics* **2024**, *13*, 1122. [CrossRef]
26. Mao, J.; Song, G.; Hao, S.; Zhang, M.; Song, A. Development of a Lightweight Underwater Manipulator for Delicate Structural Repair Operations. *IEEE Robot. Autom. Lett.* **2023**, *8*, 6563–6570. [CrossRef]
27. Antonelli, G.; Sarkar, N.; Chiaverini, S. Explicit force control for underwater vehicle-manipulator systems. *Robotica* **2002**, *20*, 251–260. [CrossRef]
28. Cui, Y.; Sarkar, N. A unified force control approach to autonomous underwater manipulation. *Robotica* **2001**, *19*, 255–266. [CrossRef]

29. Katsura, S.; Matsumoto, Y.; Ohnishi, K. Modeling of Force Sensing and Validation of Disturbance Observer for Force Control. *IEEE Trans. Ind. Electron.* **2007**, *54*, 530–538. [CrossRef]

30. Han, L.; Tang, G.; Zhou, Z.; Huang, H.; Xie, D. Adaptive wave neural network nonsingular terminal sliding mode control for an underwater manipulator with force estimation. *Trans. Can. Soc. Mech. Eng.* **2020**, *45*, 183–198. [CrossRef]

31. Phong, L.D.; Choi, J.; Kang, S. External force estimation using joint torque sensors for a robot manipulator. In Proceedings of the 2012 IEEE International Conference on Robotics and Automation, St Paul, MN, USA, 14–18 May 2012; pp. 4507–4512. [CrossRef]

32. Wahrburg, A.; Morara, E.; Cesari, G.; Matthias, B.; Ding, H. Cartesian contact force estimation for robotic manipulators using Kalman filters and the generalized momentum. In Proceedings of the 2015 IEEE International Conference on Automation Science and Engineering, Gothenburg, Sweden, 24–28 August 2015; pp. 1230–1235. [CrossRef]

33. Janiszewski, D. Load torque estimation in sensorless PMSM drive using Unscented Kalmana Filter. In Proceedings of the 2011 IEEE International Symposium on Industrial Electronics, Gdansk, Poland, 27–30 June 2011; pp. 643–648. [CrossRef]

34. Ohishi, K.; Miyazaki, M.; Fujita, M. Hybrid control of force and position without force sensor. In Proceedings of the 1992 International Conference on Industrial Electronics, Control, Instrumentation, and Automation, San Diego, CA, USA, 9–13 November 1992; pp. 670–675. [CrossRef]

35. Murakami, T.; Nakamura, R.; Yu, F.; Ohnishi, K. Force sensorless impedance control by disturbance observer. In Proceedings of the 1993 Power Conversion Conference, Yokohama, Japan, 19–21 April 1993; pp. 352–357. [CrossRef]

36. Zuev, A.V.; Filaretov, V.F. Features of designing combined force/position manipulator control systems. *J. Comput. Syst. Sci. Int.* **2009**, *48*, 154–162. [CrossRef]

37. Filaretov, V.F.; Zuev, A.V. Position-force control of the electric drive of the manipulator. *Mech. Autom. Control* **2006**, *9*, 20–24.

38. Timoshenko, A.; Zuev, A.; Filaretov, V. An approach to the construction of high-quality position force control systems for autonomous underwater vehicles with a multi-link manipulator. In Proceedings of the 2023 International Conference on Ocean Studies, Vladivostok, Russia, 3–6 October 2023; pp. 046–050. [CrossRef]

39. Taira, Y.; Sagara, S.; Oya, M. Impedance control based on error feedback for the manipulator of an underwater vehicle-manipulator system. *Artif. Life Robot.* **2023**, *28*, 830–849. [CrossRef]

40. Naghsh, A.; Sheikholeslam, F.; Danesh, M. Design of an Adaptive Fuzzy Estimator for Force/Position Tracking in Robot Manipulators. *Iran. J. Fuzzy Syst.* **2014**, *11*, 75–89. [CrossRef]

41. Ngo, V.T.; Liu, Y.C. Object transportation using networked mobile manipulators without force/torque sensors. In Proceedings of the 2018 International Automatic Control Conference, Taoyuan, Taiwan, 4–7 November 2018; pp. 1–6. [CrossRef]

42. Smith, A.C.; Mobasser, F.; Hashtrudi-Zaad, K. Neural-network-based contact force observers for haptic applications. *IEEE Trans. Robot.* **2006**, *22*, 1163–1175. [CrossRef]

43. Filaretov, V.F.; Konoplin, N.Y.; Konoplin, A.Y. System for automatic soil sampling by AUV equipped with Multilink manipulator. *Int. J. Energy Technol. Policy* **2019**, *15*, 208–223. [CrossRef]

44. Medvedev, V.S.; Leskov, A.G.; Yushchenko, A.S. *Control Systems of Manipulative Robots*; Ser. Scientific foundations of robotics; Nauka: Moscow, Russia, 1978; p. 416.

45. Popov, E.P.; Vereshchagin, A.F.; Zenkevich, S.L. *Manipulative Robots: Dynamics and Algorithms*; Nauka: Moscow, Russia, 1978; p. 398.

46. Filaretov, V.F.; Konoplin, A.Y. System of automatic stabilization of underwater vehicle in hang mode with working multilink manipulator. In Proceedings of the 2015 International Conference on Computer, Control, Informatics and Its Applications, Bandung, Indonesia, 5–7 October 2015; pp. 132–137. [CrossRef]

47. Filaretov, V.F.; Konoplin, A.Y.; Zuev, A.V.; Krasavin, N.A. A method to synthesize high-precision motion control systems for underwater manipulator. *Int. J. Simul. Model.* **2021**, *20*, 625–636. [CrossRef]

48. Pérez-Alcocer, R.; Torres-Méndez, L.A.; Olguín-Díaz, E.; Maldonado-Ramírez, A.A. Vision-based autonomous underwater vehicle navigation in poor visibility conditions using a model-free robust control. *J. Sens.* **2016**, *2016*, 1–16. [CrossRef]

49. Kostenko, V.V.; Pavin, A.M. Automatic stabilization of unmanned underwater vehicles over the seabed objects on the base of photo images. *Underw. Investig. Robot.* **2014**, *17*, 39–47.

50. Filaretov, V.; Konoplin, A. System of Automatically Correction of Program Trajectory of Motion of Multilink Manipulator Installed on Underwater Vehicle. *Procedia Eng.* **2015**, *100*, 1441–1449. [CrossRef]

51. Leabourne, K.N.; Rock, S.M. Model Development of an Underwater Manipulator for Coordinated Arm-Vehicle Control. In Proceedings of the 1998 OCEANS'98, Nice, France, 28 September–1 October 1998; pp. 941–946. [CrossRef]

52. McLain, T.W.; Rock, S.M.; Lee, M.J. Experiments in the coordinated control of an underwater arm/vehicle system. *J. Auton. Robots* **1996**, *3*, 139–158. [CrossRef]

53. Ubeda, R.P.; Gutiérrez Rubert, S.C.; Zotovic Stanisic, R.; Perles Ivars, Á. Design and Manufacturing of an Ultra-Low-Cost Custom Torque Sensor for Robotics. *Sensors* **2018**, *18*, 1786. [CrossRef] [PubMed]

54. Fossen, T.I. *Handbook of Marine Craft Hydrodynamics and Motion Control*; John Wiley & Sons: Hoboken, NJ, USA, 2011.

55. Konoplin, A.; Yurmanov, A.; Krasavin, N.; Piatavin, P.; Panchuk, M.; Vasilenko, R. System for Identifying Target Objects to Perform Manipulative Operations by Unmanned Underwater Vehicles. In Proceedings of the 2022 International Conference on Ocean Studies, Vladivostok, Russia, 5–8 October 2022; pp. 55–59. [CrossRef]

56. Jia, S.; Wang, K.; Li, X.; Xu, T. A Novel Improved Probability-Guided RANSAC Algorithm for Robot 3D Map Building. *J. Sens.* **2016**, *2016*, 1–18. [CrossRef]

57. Liu, H.; Song, R.; Zhang, X.; Liu, H. Point cloud segmentation based on Euclidean clustering and multi-plane extraction in rugged field. *Meas. Sci. Technol.* **2021**, *32*, 095106. [CrossRef]

58. Wang, F.; Zhao, Z. A survey of iterative closest point algorithm. In Proceedings of the 2017 Chinese Automation Congress, Jinan, China, 20–22 October 2017; pp. 4395–4399. [CrossRef]

59. Konoplin, A.Y.; Pyatavin, P.A. Method of Autonomous Implementation of Manipulation Operations with Underwater Objects Having Predetermined Shape. In Proceedings of the 2021 International science and technology conference "Earth science", Vladivostok, Russia, 8–10 December 2020; p. 042083. [CrossRef]

60. Kostenko, V.V.; Bykanova, A.Y.; Tolstonogov, A.Y. Developing the Multilink Manipulator System for an Autonomous Underwater Vehicle. In Proceedings of the 2022 International Conference on Ocean Studies, Vladivostok, Russia, 5–8 October 2022; pp. 45–50. [CrossRef]

61. Borovik, A.I.; Rybakova, E.I.; Galkin, S.V.; Mikhailov, D.N.; Konoplin, A.Y. Experience of Using the Autonomous Underwater Vehicle MMT-3000 for Research on Benthic Communities in Antartica. *Oceanology* **2022**, *62*, 709–720. [CrossRef]